

Protease-resistant modified human β -hexosaminidase B ameliorates symptoms in GM2 gangliosidosis model

Keisuke Kitakaze,¹ Yasumichi Mizutani,¹ Eiji Sugiyama,² Chikako Tasaki,¹ Daisuke Tsuji,¹ Nobuo Maita,³ Takatsugu Hirokawa,⁴ Daisuke Asanuma,⁵ Mako Kamiya,⁶ Kohei Sato,⁷ Mitsutoshi Setou,^{2,8,9,10} Yasuteru Urano,^{5,6} Tadayasu Togawa,¹¹ Akira Otaka,⁷ Hitoshi Sakuraba,¹² and Kohji Itoh¹

¹Department of Medicinal Biotechnology, Institute for Medicinal Research, Graduate School of Pharmaceutical Science, Tokushima University, Tokushima, Japan. ²Department of Cell Biology and Anatomy, Hamamatsu University School of Medicine, Shizuoka, Japan. ³Laboratory of X-ray Crystallography, Institute for Enzyme Research, Tokushima University, Tokushima, Japan. ⁴Molecular Profiling Research Center for Drug Discovery (molprof), National Institute of Advanced Industrial Science and Technology (AIST), Tokyo, Japan. ⁵Laboratory of Chemistry and Biology, Graduate School of Pharmaceutical Sciences, and ⁶Laboratory of Chemical Biology and Molecular Imaging, Graduate School of Medicine, The University of Tokyo, Tokyo, Japan. ⁷Department of Bioorganic Synthetic Chemistry, Graduate School of Pharmaceutical Science, Tokushima University, Tokushima, Japan. ⁸Division of System Molecular Anatomy, Medical Photonics Research Center, Hamamatsu University School of Medicine, Shizuoka, Japan. ⁹The Institute of Medical Science, The University of Tokyo, Tokyo, Japan. ¹⁰Department of Anatomy, The University of Hong Kong, Pok Fu Lam, Hong Kong, China. ¹¹Department of Functional Bioanalysis and ¹²Department of Clinical Genetics, Meiji Pharmaceutical University, Tokyo, Japan.

GM2 gangliosidoses, including Tay-Sachs and Sandhoff diseases, are neurodegenerative lysosomal storage diseases that are caused by deficiency of β -hexosaminidase A, which comprises an $\alpha\beta$ heterodimer. There are no effective treatments for these diseases; however, various strategies aimed at restoring β -hexosaminidase A have been explored. Here, we produced a modified human hexosaminidase subunit β (HexB), which we have termed mod2B, composed of homodimeric β subunits that contain amino acid sequences from the α subunit that confer GM2 ganglioside-degrading activity and protease resistance. We also developed fluorescent probes that allow visualization of endocytosis of mod2B via mannose 6-phosphate receptors and delivery of mod2B to lysosomes in GM2 gangliosidosis models. In addition, we applied imaging mass spectrometry to monitor efficacy of this approach in Sandhoff disease model mice. Following i.c.v. administration, mod2B was widely distributed and reduced accumulation of GM2, asialo-GM2, and bis(monoacylglycero) phosphate in brain regions including the hypothalamus, hippocampus, and cerebellum. Moreover, mod2B administration markedly improved motor dysfunction and a prolonged lifespan in Sandhoff disease mice. Together, the results of our study indicate that mod2B has potential for intracerebrospinal fluid enzyme replacement therapy and should be further explored as a gene therapy for GM2 gangliosidoses.

Introduction

GM2 gangliosidoses, including Tay-Sachs disease (TSD, OMIM 272800), Sandhoff disease (SD, OMIM 268800), and GM2 ganglioside activator protein (GM2A) deficiency (variant AB, OMIM 272750), are neurodegenerative lysosomal storage diseases (LSDs) associated with excessive accumulation of GM2 in the brain, which leads to neurological symptoms (1). TSD and SD are autosomal recessive lysosomal β -hexosaminidase A (HexA) deficiencies caused by gene mutations in *HEXA* and *HEXB*, respectively encoding the α - and β subunits of HexA ($\alpha\beta$ heterodimer). The underlying mechanism of the neuropathogenesis is still unclear, although it has been reported that lysosomal accumulation of their substrates, including glycosphingolipids, oligosaccharides, and glycosaminoglycans, leading to inflammatory responses (microglial activation and astrogliosis) and neuronal injury are the hallmarks during the course of these disorders (1, 2). There are currently no effective treatments for GM2 gangliosidoses,

although several therapeutic approaches have been developed, including gene therapy (GT) (2, 3), enzyme replacement therapy (ERT) (4, 5), substrate reduction therapy (SRT) (6, 7), and pharmacological chaperone therapy (PCT) (8). An SD model mouse was generated by targeted disruption of the *Hexb* gene allele (9, 10) and was utilized for investigating the neuropathogenic mechanism and evaluating the therapeutic approaches as an authentic infantile GM2 gangliosidosis model, which develops the pathological features — including spasticity, muscle weakness, rigidity, tremor, and ataxia — that closely resemble those observed in the acute form of human disorders.

We previously established intracerebroventricular ERT (i.c.v.ERT) for neurodegenerative SD model mice using the methylotrophic yeast-derived human HexA (*Om4HexA*) with a high content of terminal mannose 6-phosphate (M6P) residues and demonstrated the importance of uptake by neural tissues via the cell surface cation-independent M6P receptor (CI-M6PR) (11) system in suppressing the neuroinflammation and treating the neurological symptoms (4). We also evaluated the reduction of the GM2 and asialo-GM2 (GA2) accumulation in the brain parenchyma by conventional TLC and immunohistochemical methods (4). How-

Conflict of interest: The authors have declared that no conflict of interest exists.

Submitted: November 19, 2015; **Accepted:** February 9, 2016.

Reference information: *J Clin Invest.* 2016;126(5):1691–1703. doi:10.1172/JCI85300.

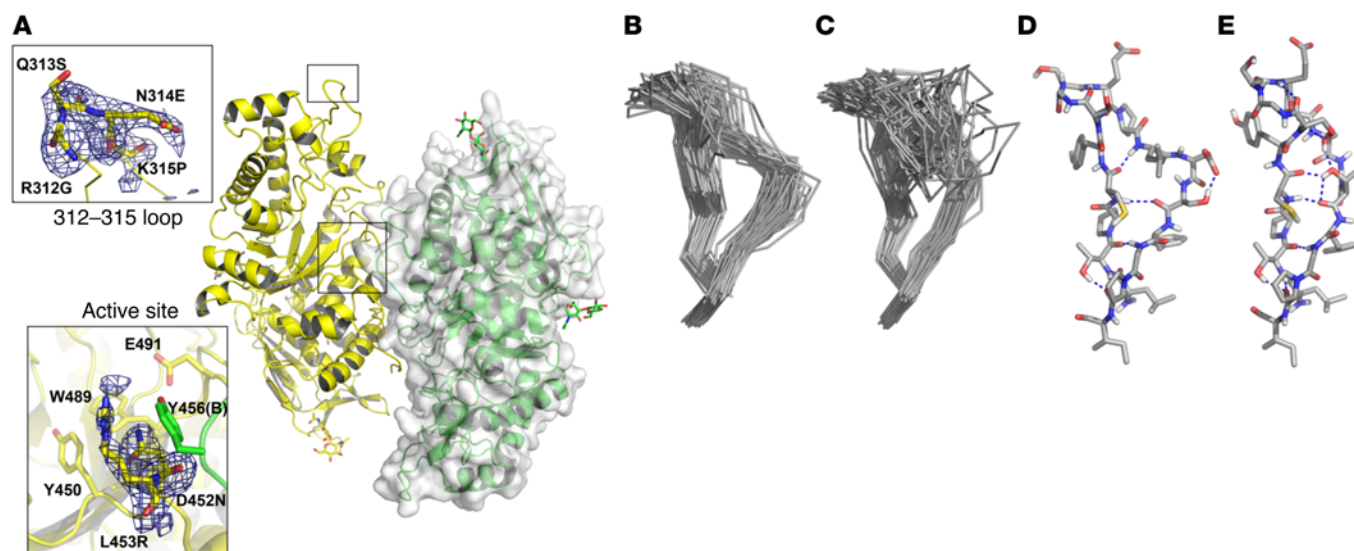


Figure 1. Crystal structure of human modB and the predicted model for mod2B. (A) Overall structure of the modB dimer determined at 2.4 Å. A close-up view of the β_1 312–315 loop, and the active site residues are shown in insets. The electron densities of the omit map (contoured at 2σ) around the modified sites are also shown. (B–E) Structure of the GSEP loop region of modB and mod2B. Structural snapshots of the GSEP loop region of modB (B) and mod2B (C) from MD trajectories taken every 1 ns. The amino acid regions from 307–322 including the GSEP loop, are shown with ribbon models. Representative structures of the GSEP loop regions of modB (D) and mod2B (E) are shown in stick models. All nonpolar hydrogen atoms are omitted for clarity. Hydrogen bonds within the GSEP loop regions are depicted by blue dashed lines.

ever, few simple and effective methods have been developed for monitoring therapy in animal models of neurodegenerative LSDs.

In this study, we show the production of a modified and protease-resistant HexB (mod2B) using a Chinese hamster ovary (CHO) cell line overexpressing single human modified *HEXB* cDNA that contained additional α sequences near the GM2A binding loop and compared it with the previous modified HexB (modB) (5) with GM2A-binding and GM2-degrading activities in vivo. Furthermore, we not only propose a fluorescent substrate for the vital imaging of Hex activity in culture and in situ, but we also apply an acidic pH-activatable fluorescent probe (12, 13) for visualization of recombinant enzyme uptake by cultured cells and delivery to acidic compartments (late endosomes/lysosomes). We also propose the successful application of an imaging mass spectrometry (IMS) system (14–16) to identify substrates and substances — including GM2, GA2, and bis(monoacylglycero)phosphate (BMP) (17, 18), which accumulate in the brains of SD mice — and we can monitor their reduction during the modified HexB replacement closely correlated with the effectiveness. We herein show that i.c.v. administration of mod2B with superior biostability and bioavailability to modB had remarkably excellent therapeutic effects on SD mice.

Results

Molecular design and properties of the human modified HexBs. We previously designed modB (5), which contains a partial amino acid sequence of the α subunit based on homology modeling using the crystal structures of human HexA ($\alpha\beta$ heterodimer, Protein Data Bank [PDB] ID: 2GJX) (19) and HexB ($\beta\beta$ homodimer, PDB ID: 1NOU) (20). We replaced the 2 amino acids DL (β 452–453) with NR (α 423–424), which are necessary for anionic substrate recognition in the α subunit. We also replaced the RQNK (β 312–315) sequence

with GSEP (α 280–283), which is required for the interaction with GM2A, an essential cofactor for GM2 degradation (21, 22). The modB is composed of the homodimeric modified β subunits (β_1') secreted by a CHO cell line, which retained thermostability similar to that of human HexB in vitro and could reduce the GM2 and GA2 accumulation in the brains of SD mice following i.c.v. administration (5). In this study, we elucidated the x-ray crystal structure of purified modB (newly registered PDB ID: 5BRO), which retained a local conformation of the active pocket of β_1' subunits very similar to that of the α subunits and the introduced GSEP loops (Figure 1A and Supplemental Figure 1; supplemental material available online with this article; doi:10.1172/JCI85300DS1).

We herein designed and produced a human modified HexB2 (mod2B) composed of β_2' , in which the LDS (β 316–318) sequence was further replaced with SGT (α 284–286) because it putatively protected the GSEP loop sequence from proteolytic degradation. We compared and summarized the amino acid sequence substitutions, enzymatic properties, and therapeutic functions of the human modified HexBs (modB and mod2B), as well as HexA and HexB (refs. 4, 5, 22–26, and Table 1).

We purified the modB and mod2B with terminal M6P-containing *N*-glycans by 3-step column chromatography (Supplemental Table 1), including an affinity chromatography step with Phos-tag resin, which is usually used to capture phosphorylated proteins (27). The modB and mod2B purified from the serum-free conditioned medium (CM) were both composed of the precursor forms (β_1' -P and β_2' -P) and the mature forms (β_1' -M and β_2' -M) as determined by SDS-PAGE under reducing conditions (Supplemental Figure 2, A–C). Note that the mod2B exhibited potent GM2-degrading activity in cooperation with the synthetic GM2A (28), as with HexA, but the modB had less activity in vitro (Supplemental Figure 2D).

Table 1. Comparison of enzymatic properties and functions among Hex isozymes

Hex isozyme (name)	mod2B	modB	HexB	HexA
Gene	modified <i>HEXB</i>	modified <i>HEXB</i>	<i>HEXB</i>	<i>HEXA/HEXB</i>
Amino acid substitutions in β subunit	RQNK 312–315 GSEP, LDS 316–318 SGT, DL 452–453 NR	RQNK 312–315 GSEP, DL 452–453 NR	–	–
Subunit composition (dimer)	$\beta_2'\beta_2'$	$\beta_1'\beta_1'$	$\beta\beta$	$\alpha\beta$
Molecular species detected on immunoblotting under reducing conditions (kDa)	β_2' -P (63), β_2' -M (51)	β_1' -P (63), β_1' -M (51), β_1' -PD (25)	β -P (63), β -M (29)	α -P (67), α -M (54), β -P (63), β -M (29)
Natural substrate	GM2, GA2, β GlcNAc-R	GM2, GA2, β GlcNAc-R	β GlcNAc-R	GM2, GA2, β GlcNAc-R
Artificial substrate	MUG, MUGS	MUG, MUGS	MUG	MUG, MUGS
Specific activity toward MUGS ($\mu\text{mol min}^{-1} \text{mg}^{-1}$)	12.6	10.3	0.05	8.3
K_m (mM)/ V_{max} (mol min ⁻¹ mg ⁻¹) for MUGS	0.32/5.8 $\times 10^{-5}$	0.34/5.7 $\times 10^{-5}$	3.4/1.2 $\times 10^{-6}$	0.31/2.5 $\times 10^{-5}$
Thermostability at 37°C in vitro ($t_{1/2}$) (Supplemental Figure 2E)	> 1 wk	> 1 wk	> 1 wk	< 2 d
Intracellular half-life ($t_{1/2}$)	10.7 d	11.6 d	ND	6.6 d
M6P-type N-glycan/N-glycan	4/8	4/8	4/8	3/7
M6P contents (mol/mol Hex)	5.6 \pm 0.3	5.1 \pm 0.6	ND	ND
Crystal structure (PDB ID)	ND (in silico prediction)	5BRO (Figure 1A)	1NOU	2GJX
In vitro degradation of GM2 in the presence of GM2A (Supplemental Figure 2D)	++	+	–	++
Intracellular GM2-degrading activity	+	+	–	+
GM2-degrading activity in vivo	++	+	– (DNS)	++
Improvement of rota-rod performance	+	–	– (DNS)	+
Prolongation of lifespan	+	–	– (DNS)	+

DNS, data not shown.

We also predicted the structure of mod2B (Figure 1, B–E) based on the crystal structure of modB (PDB ID: 5BRO) (Supplemental Table 2) and human HexA (PDB ID: 2GJX). The results of the trajectory analysis from a molecular dynamics (MD) simulation showed that the average pairwise root-mean-square deviation (RMSD) of the GSEP loop regions of modB and mod2B were 2.315 Å and 3.869 Å, respectively. S318 forms a hydrogen bond with D317 in modB, whereas S311, S316, and T318 form hydrogen bonds in the structural core area with S316, T318, and C309, respectively, in mod2B (Figure 1, D and E). These MD simulation results suggest that the GSEP loop region is more flexible in mod2B than in modB.

Lysosomal enzyme delivery and GM2 reduction in patient cells.

We added the purified modB and mod2B to the cultured medium of fibroblasts derived from a TSD patient (F218) (26) and an SD patient (F572) (5). Significant restoration of the MUGS-degrading activity in the extract of SD fibroblasts was observed 4 days after treatment with either modB or mod2B. The significant inhibition of the recovery of intracellular β -Hex activity in the presence of 5 mM M6P indicated that both modB and mod2B were taken up via the cell surface CI-M6PR (Figure 2A). We succeeded in performing the vital imaging of the intracellular β -Hex activity caused by the endocytosed modB and mod2B using a fluorescent substrate, HMDER- β GlcNAc (Supplemental Figure 3, A–C). When we incubated cultured fibroblasts derived from a normal subject and the SD patient with HMDER- β GlcNAc, punctate fluorescence was observed in normal cells, while no obvious fluorescence was seen in SD fibroblasts, which have no endogenous β -Hex activity. In

contrast, we observed remarkable fluorescence in SD fibroblasts 24 hours after treatment with modB or mod2B (Figure 2B).

We also visualized the enzyme delivery to lysosomes in living cells with a pH-activatable fluorescent probe, AcidiFluor ORANGE (AFO) (13). We prepared the conjugates (AFO-modB and -mod2B) and then added them to the culture medium of SD fibroblasts. We observed remarkable fluorescence colocalized with lysosome-associated membrane protein 1 (LAMP1) in SD fibroblasts 24 hours after treatment with the AFO-modB or -mod2B. However, in the presence of 5 mM M6P in culture medium, little fluorescence was detected (Figure 2C and Supplemental Figure 4). There seemed to be little difference between modB and mod2B in terms of the intracellular uptake via CI-M6PR, likely because the contents of the terminal M6P residues of the 2 enzymes are relatively similar and the intracellular half-life ($t_{1/2}$) values evaluated by MUGS-degrading activity disappearance in cultured fibroblasts derived from patients were 11.6 days for modB and 10.7 days for mod2B, respectively (Table 1).

We also evaluated the GM2-degrading activity of modB and mod2B in the culture system. Cultured TSD fibroblasts were treated with modB or mod2B for 7 days, then examined by immunostaining with Ab against GM2 (29). We detected excessive accumulation of GM2 as punctate fluorescence (green) in untreated TSD fibroblasts. After treatment with modB or mod2B, the punctate fluorescence due to GM2 was reduced. In contrast, immunofluorescence (red) for human Hex proteins with a human HexA-specific Ab (30) was observed separately from the GM2

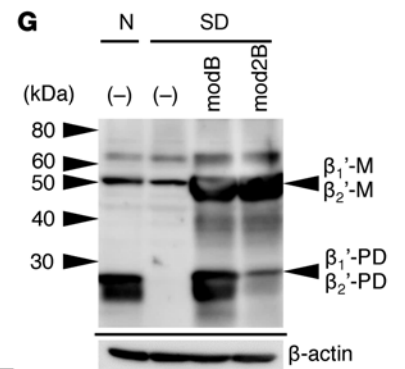
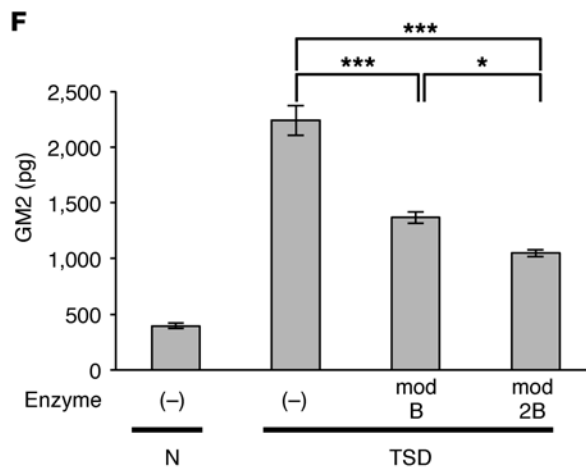
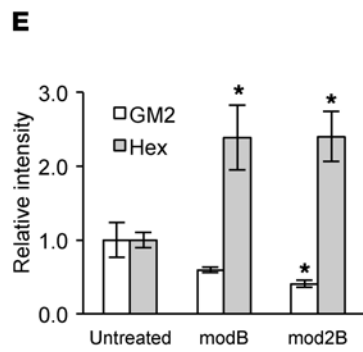
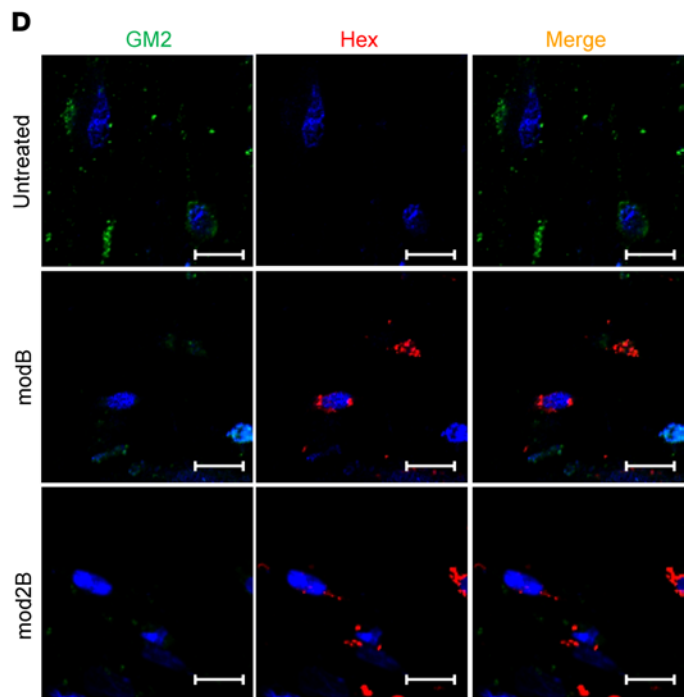
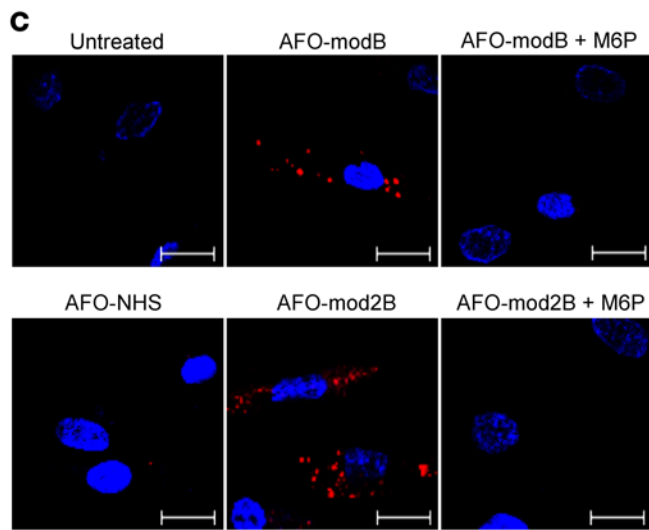
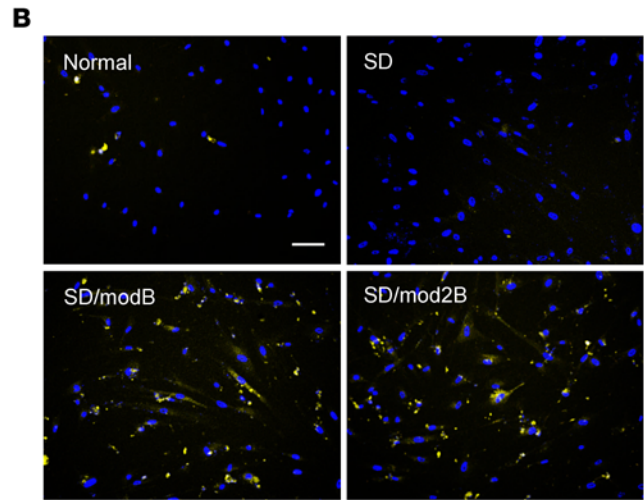
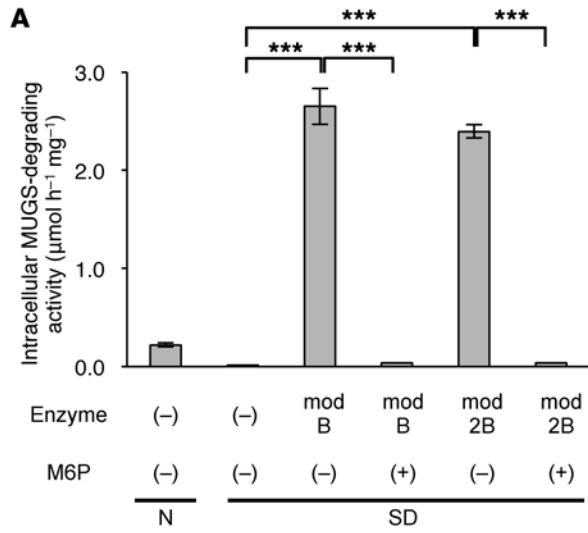


Figure 2. Recombinant enzyme replacement in cultured human fibroblasts derived from patients with GM2 gangliosidosis. (A) Intracellular MUGS-degrading activity in SD fibroblasts after treatment with modB or mod2B. Before enzyme treatment, fibroblasts were treated (+) or not treated (-) with M6P. Error bars show mean \pm SEM ($n = 3$). ANOVA with a Tukey post-hoc test; *** $P < 0.001$. (B) Vital staining of the β -Hex activity with HMDER- β GlcNAc. SD fibroblasts were treated with modB or mod2B, followed by incubation with HMDER- β GlcNAc. Blue, nuclei; yellow, HMDER. Scale bar: 100 μ m. (C) Hex delivery imaging. AFO-modB, AFO-mod2B, or AFO-NHS was added to SD fibroblasts. Living cells were viewed with a confocal fluorescent microscope. Blue, nuclei; red, AFO. Scale bars: 20 μ m. (D and E) TSD fibroblasts were treated with modB or mod2B and immunostained for GM2 (green) and Hex proteins (red), and relative contents were examined by confocal laser scanning microscopy. Scale bars: 20 μ m. Error bars show mean \pm SEM ($n = 6-7$). ANOVA with a Tukey post-hoc test; * $P < 0.05$. (F) GM2-ELISA. TSD fibroblasts were treated with modB or mod2B to evaluate the intracellular GM2-degrading activity. Error bars show mean \pm SEM ($n = 7$). ANOVA with a Tukey post-hoc test; * $P < 0.05$, *** $P < 0.001$. (G) The protease sensitivities of modB and mod2B incorporated in SD fibroblasts. Immunoblotting of cell extracts with anti-NAG(A) after enzyme replacement. β -Actin blot is from duplicate samples run on a parallel gel. Each lane contained 7.5 μ g of protein.

accumulated in the modB-treated TSD fibroblasts (Figure 2, D and E), indicating that there was GM2 degradation in the lysosomes containing modified HexBs. More potent GM2-degrading activity of mod2B compared with modB was also shown by GM2-ELISA (ref. 31 and Figure 2F). In addition, there was a higher content of the 51-kDa mature form (M) compared with the 25-kDa proteolytically degraded product (PD) in SD fibroblasts when they were treated with mod2B than with modB for 4 days (Figure 2G).

Protease resistance of mod2B injected into SD mouse brain. Next, we evaluated the effects of i.c.v. enzyme replacement using the modified HexBs in SD mice following administration when they were 10 weeks old. One week after i.c.v. injection of modB or mod2B, the MUGS-degrading activity was significantly restored in both the brains and peripheral organs of the mice (Supplemental Figure 5, A-C). The distribution of human modified HexBs in the hippocampal formation detected by immunostaining indicated that the modB and mod2B injected into the cerebrospinal fluid (CSF) were incorporated into neural cells of the brain parenchyma (Figure 3A). In situ β -Hex activity imaging with the fluorogenic substrate, HMDER- β GlcNAc, also showed a wide distribution and restoration of β -Hex activity following incorporation in brain parenchymal cells throughout the brain, including the thalamus, hippocampus (HIP), hypothalamus (HY), and cerebellum (CB) (Supplemental Figure 5D). Immunoblotting with an human HexA-specific Ab revealed that the modB taken up by parenchymal neural cells was processed to the 25-kDa PD from the 46-kDa M, while the mod2B was present mainly as the 46-kDa M, though there was a little of the 25-kDa PD, as well (Figure 3, B and C). These results clearly indicated that the intralysosomal mod2B is more resistant to neural proteases than modB, and the α -type loop sequence, SGT (β_2 '316-318) — in addition to the GSEP (β_1 '312-315) — was considered to improve the protease resistance of the mature mod2B as well as HexA, which is necessary for maintenance of the intralysosomal GM2-degrading activity in cooperation with GM2A.

Lipid reduction in SD mouse brains by i.c.v. injection of mod2B. To evaluate the effects of modB and mod2B on the lipid accumulation in SD mouse brains, we applied a matrix-assisted laser

desorption/ionization IMS (MALDI-IMS) system and detected remarkable signals corresponding to GM2 and GA2 in untreated 11-week-old SD mice, while these were hardly detected in untreated 11-week-old WT mice. We also performed tandem mass spectrometry (MS/MS) on tissue sections to validate the results for each molecular species (Supplemental Figure 6, A-H). We observed GM2 (d18:1/18:0) mainly in the HY, lateral septal nucleus (LSN), and HIP; the expression of GM2 (d20:1/18:0) was marked in the CB (Figure 4A). We also observed GA2 (d18:1/18:0) and GA2 (d20:1/18:0) throughout the brain (Figure 4B). We noted that BMP (d22:6/22:6) (17, 18) accumulated especially in the CB of SD mice, which is the first evidence of this accumulation detected by IMS. The accumulated BMP was also reduced by treatment with modified HexBs (Figure 4A). Importantly, treatment with mod2B decreased the signals of GM2, GA2, and BMP more efficiently than modB in all brain regions, including the CB and LSN (Figure 4, A-D, and Supplemental Figure 7, A-H).

Therapeutic effects of i.c.v. injection of the mod2B on SD mice. SD mice present an age-dependent onset of severe motor dysfunction (9, 10). We herein evaluated the long-term therapeutic effects of i.c.v. administration beginning at 10 weeks of age. Following a single i.c.v. administration (1 mg/kg body weight [BW] dose), the mod2B-treated SD mice exhibited more improved rota-rod performance than PBS-treated mice. Repeated i.c.v. injection (twice at a 2-week interval, 2 mg/kg BW dose each time) of mod2B also significantly prolonged the mean time on the rota-rod (Figure 5A). The mean lifespans of the SD mice treated with PBS, a 1 mg/kg or a 2 mg/kg BW dose of modB, or a 1 mg/kg or a 2 mg/kg BW dose of mod2B were 123.2, 128.8, 125.3, 126.7, and 156.5 days, respectively (Figure 5B). The BWs of the SD mice treated twice with mod2B were maintained at 14 and 16 weeks of age (Supplemental Figure 8). These results showed that mod2B had more potent therapeutic effects than modB, likely due to the better resistance to proteases and the relatively longer half-life of GM2-degrading activity of mod2B in neural cells.

Discussion

The unmet medical needs for developing therapy for the neurodegenerative LSDs has been increasing, since the intravenous ERT (i.v.ERT) with recombinant human lysosomal enzymes produced by CHO and human HT1080 cell lines has been clinically applied for several LSDs involving peripheral and visceral manifestations (32), which have limited therapeutic effects on neurological symptoms because of the presence of blood-brain barrier (BBB). In recent years, preclinical studies (33, 34) and clinical trials of intrathecal ERT (i.t.ERT) and i.c.v.ERT in the USA have been making steady progress for neurodegenerative LSDs, including mucopolysaccharidosis (MPS) type I (phase 1) (35), II (phase 2/3) (36), and IIIA (phase 2); Batten disease (phase 1/2); and metachromatic leukodystrophy (MLD) (phase 1/2) (according to ClinicalTrials.gov, <https://clinicaltrials.gov/>, accessed July 1, 2015). Novel approaches with BBB-penetrating tags have also been attempted in animal disease models (37). Intracerebral GT using adeno-associated virus (AAV) vectors for MPS IIIA (phase 1/2) (38) and MLD (phase 1/2) has been also evaluated in Europe (according to ClinicalTrials.gov), which is feasible to be clinically applied, although the adverse effects of irreversible gene transfer to the patients may

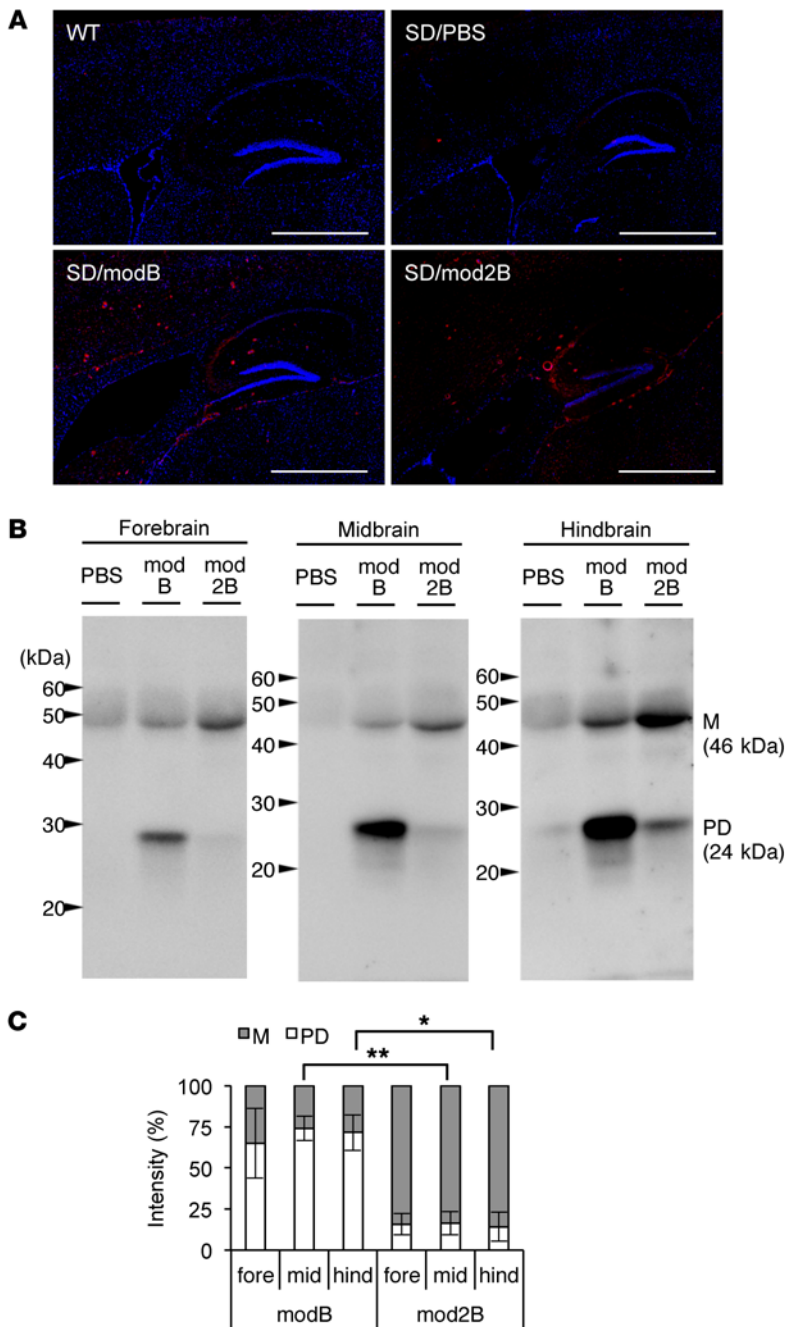


Figure 3. Distribution and protease sensitivities of modified HexBs in SD mouse brains after i.c.v. administration.

(A) Immunohistochemical analyses of Hex proteins with anti-NAG(A) in the hippocampal formation of SD mice treated with modB or mod2B (5 mg/kg BW dose). Blue, nuclei; red, Hex proteins. Scale bars: 1 mm. (B and C) Protease sensitivities of modB and mod2B in SD mouse brains. IP and immunoblotting of brain extracts with human HexA-specific Ab. Error bars show mean \pm SEM ($n = 3$). Unpaired t test; * $P < 0.05$, ** $P < 0.01$. M = 46 kDa; PD = 24 kDa.

LDS to SGT as the normal human α subunit does; as the mod2B similar to HexA ($\alpha\beta$ heterodimer) exhibited more potent GM2-degrading activity in cooperation with synthetic GM2A in vitro than modB (Supplemental Figure 2D), there are structural advantages of the GSEPSGT loop of mod2B, which is predicted to be more flexible in the interaction with the GM2/GM2A complex than the GSEPLDS loop of modB. The recombinant mod2B similar to HexB ($\beta\beta$ homodimer) is more thermostable at 37°C than normal human HexA in vitro; that is advantageous in manufacturing as well as in in vivo stability after administration. The numbers of terminal M6P-containing N -glycans attached to mod2B (4/1 homodimeric molecule) are greater than those of HexA (3/1 heterodimeric molecule). The incorporation of mod2B through its binding with cell surface CI-M6PR is also expected to be more efficient than that of HexA in vivo. The $t_{1/2}$ values of HexA, modB, and mod2B were 6.6 days, 11.6 days, and 10.7 days, respectively, in cultured fibroblasts derived from patients with GM2 gangliosidosis, as shown in Table 1. The $t_{1/2}$ of *Om4HexA* in the brains of Sandhoff mice was 4–6 days after i.c.v. administration (D. Tsuji, unpublished observations). These results suggest that the $t_{1/2}$ values of modB and mod2B should be relatively longer than those of the native human HexA. We herein demonstrated that repeated administration by i.c.v.ERT using mod2B had remarkable therapeutic effects, including improvement of the motor dysfunction and life extension of SD model mice. This was caused by the incorporation of the therapeutic molecule via neural cell surface CI-M6PR, followed by delivery to lysosomes and a reduction of the accumulated substrates, as supported by our previous studies

still be possible. In this study, we first constructed a human modified *HEXB* encoding the modified β_2 -P containing the additional α -type amino acid sequence, SGT (β_2 '316–318, corresponding to α 284–286) instead of LDS (β 316–318), compared with those of the modB previously reported (5), and we produced the recombinant human mod2B by a CHO cell line stably expressing the modified *HEXB*. We then analyzed their molecular properties and examined their biological effects. As summarized in Table 1, the purified mod2B composed of the modified β_2 '-precursor homodimers carrying terminal M6P-containing N -glycans has great advantages as a therapeutic gene product for TSD and SD. It can degrade not only natural substrates, including GM2 and GA2, but it also exhibits protease resistance due to the amino acid substitution of

ies (4, 5, 26) in addition to the in vivo stability due to the protease resistance in the brain parenchyma. The GSEPLDS loop structure of modB may be cleaved by lysosomal endoproteases, possibly cathepsins L and B, after being incorporated and delivered to lysosomes because the proteolytic cleavage was inhibited by pretreatment of the microglial cells derived from SD mouse brain with leupeptin, a thiol protease inhibitor for cathepsins L and B (data not shown), although the enhancement of intracellular GM2 degradation by the modB replacement should be proved under the conditions in which the endoprotease activities are inhibited.

Another recent problem associated with i.v.ERT is the production of neutralizing Ab that inhibit the uptake of the administered enzymes by target organs or that inhibit the functions of the enzyme

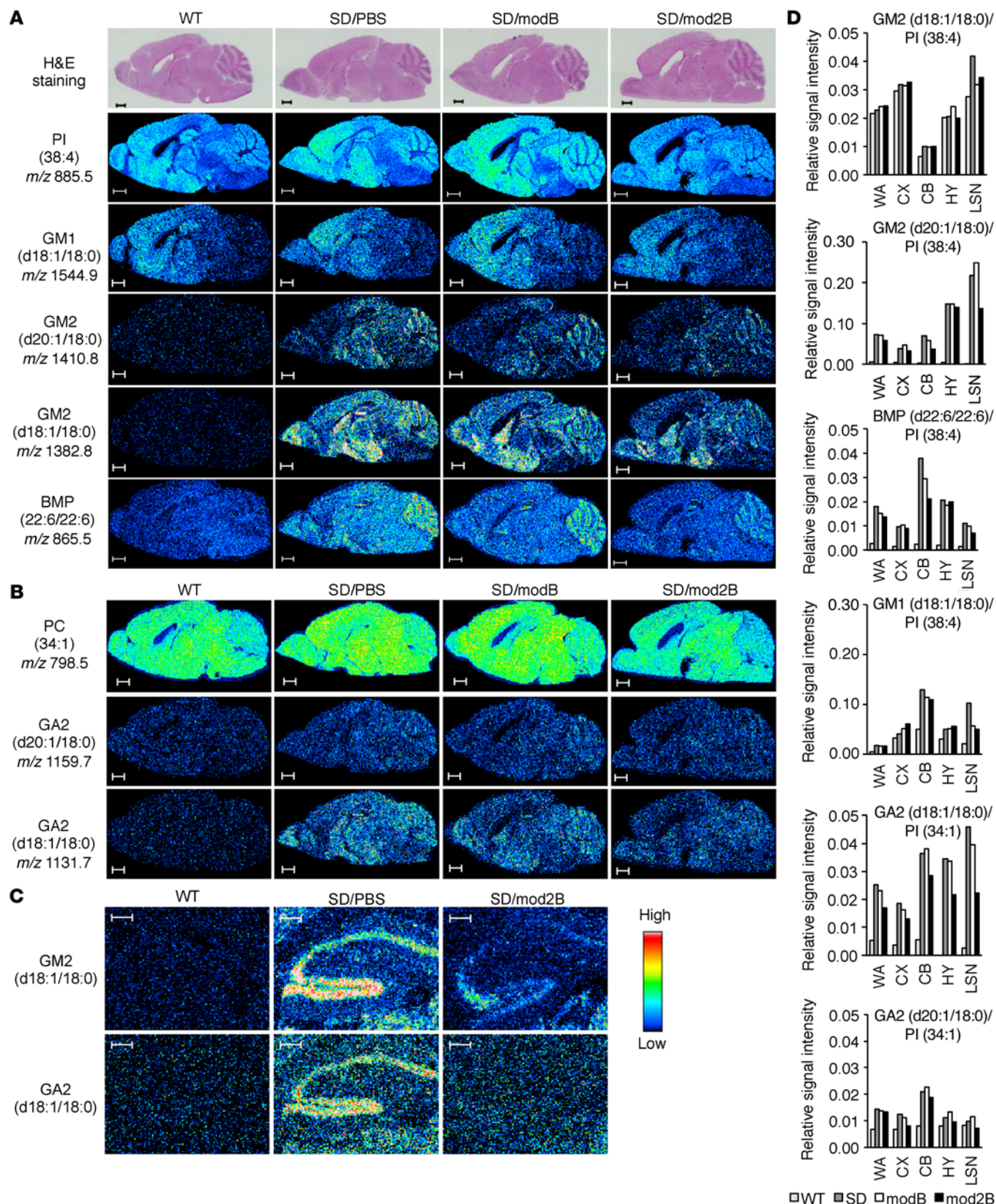


Figure 4. Lipid accumulation in brain sections of SD mice visualized by IMS. (A and B) The brains of 11-week-old WT and SD mice treated with PBS, modB, or mod2B (1 mg/kg BW dose) were examined in negative (A) and positive (B) ion modes. Scan pitch: 70 μ m. Scale bars: 1 mm. GM1, GM1 ganglioside. (C) The hippocampal formation of GM2 (d18:1/18:0) and GA2 (d18:1/18:0) in the 11-week-old WT and SD mice treated with PBS or mod2B (1 mg/kg BW dose). Scan pitch: 10 μ m. Scale bars: 200 μ m. (D) Relative signal intensities of GM2, BMP, GM1, and GA2 in each brain area. WA, whole area; CX, cerebral cortex.

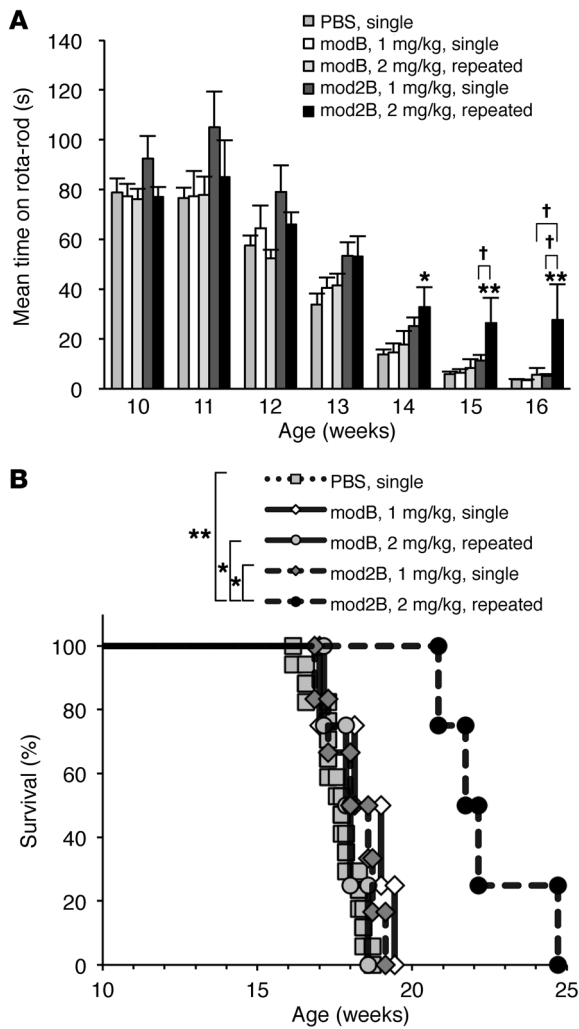


Figure 5. Long-term therapeutic effects after i.c.v. administration. (A) Evaluation of the motor dysfunction. PBS, modB, or mod2B was singly (1 mg/kg BW) or repeatedly (2 mg/kg BW, twice at a 2-week interval) administered to SD mice by i.c.v. injection. Error bars show mean \pm SEM (PBS, $n = 11$; modB single, $n = 4$; modB repeated, $n = 4$; mod2B single, $n = 6$; mod2B repeated, $n = 4$). ANOVA with a Tukey post-hoc test; * $P < 0.05$, ** $P < 0.01$ (vs PBS-treated control); † $P < 0.05$. **(B)** The results of a lifespan analysis. Single i.c.v. injections of modB ($n = 4$) and mod2B ($n = 6$), and repeated i.c.v. injections of modB ($n = 4$), had no significant effect on the lifespan compared with the PBS-treated control ($n = 17$). Repeated i.c.v. injection of mod2B ($n = 4$) significantly prolonged the lifespan (log-rank test) compared with the PBS-treated control.

nogenicity of the modified NAGA has been evaluated by utilizing a human NAGA-transgenic *Gla* KO mouse, and i.v. administration of the modified NAGA did not induce immune response to it in the NAGA-transgenic *Gla* KO mice (H. Sakuraba, unpublished observations). These findings may suggest the low antigenicity of mod2B toward TSD (Hex α -subunit deficiency).

Recently, Cachón-González et al. demonstrated that the nature of the neurological injury in the SD mouse due to accumulation of glycoconjugates, lipids, α -synuclein, and ubiquitinated proteins — and induction of inflammatory responses and neuronal loss — (2) could be reversed by intracranial delivery of recombinant AAV vectors expressing the human HexA ($\alpha\beta$) injected into striatum and CB, but also demonstrated that defects in myelination occurring in the early asymptomatic stage cannot be easily resolved when treatment is given at a later stage (2). These findings suggest the importance of the early events during the course of pathogenesis of GM2 gangliosidosis and the start time of GT. However, the newly synthesized HexAs in the brain parenchymal cells are still immunogenic for TSD patients, although cross-correction effects of recombinant human HexA secreted from neural cells are expected. In contrast, a modified *HEXB* cDNA singly encoding the modified Hex β subunit should be a useful therapeutic gene for intracranial or intranasal GT for TSD and SD patients. Moreover, a modified Hex β subunit can be applied at earlier stages before onset of neurological signs and symptoms. Sinici et al. also discussed the availability of single GT for GM2 gangliosidosis with AAV vector encoding the modified Hex β subunit (43). We would also expect the long-lasting therapeutic effect of gene transfer with AAV vector containing our mod2B cDNA because the mod2B as gene products should have protease-resistant GM2-degrading activity and relatively longer $t_{1/2}$ than HexA in brains.

From the view point of the pathogenic mechanisms of neurodegenerative diseases, Cuervo and colleagues demonstrated the impairment of lysosomal degradation of α -synuclein and leucine-rich repeat kinase 2 (LRRK2) by chaperone-mediated autophagy (CMA) in the brains of familial Parkinson’s disease (PD) patients — a neurodegenerative motor disorder characterized by the presence of α -synuclein-containing Lewy Body inclusions — and LRRK2-transgenic mice (44), and they suggest that dysregulation of cellular proteostasis of α -synuclein and ubiquitinated proteins is due to alterations in the ubiquitin-proteasome and the autophagic-lysosomal systems (45). Xiao et al. demonstrated that reduction of steady-state levels of amyloid precursor protein (APP), resulting in decreased interstitial fluid A β levels and attenuated amyloid deposits in the brains of Alzheimer’s disease

drugs in LSD patients because of the need for continuous administration of the therapeutic enzymes in the patients (39). Therefore, non/low-antigenic therapeutic enzymes are required for continuous ERT for LSDs to avoid allergic and immune responses in the patients. To meet this need, we designed modified Hex β subunits containing as few amino acid sequences of the α subunit as possible (6 in modB and 9 residues in mod2B) but which still exhibited GM2-degrading activity in vivo. In TSD patients, the endogenous HexB isozymes ($\beta\beta$ homodimer) are normally expressed, although HexA ($\alpha\beta$ heterodimer) and HexS ($\alpha\alpha$ homodimer) are absent due to the Hex α subunit deficiency. Therefore, the “camouflaged” HexBs (modB and mod2B) composed of the modified β subunits retaining almost the same amino acid sequences as the normal Hex β subunit (compared with normal HexA) are expected to be low-antigenic therapeutic enzymes that can be used for TSD patients. We predicted the immunogenicity of the altered amino acid sequences in mod2B compared with that of the native human Hex β subunit by utilizing prediction programmes NetMHC (40) and SYFPEITHI (41). We could not predict remarkably strong antigenic sequences in the altered mod2B using these programs. Previously, we also developed a human modified α -N-acetylgalactosaminidase A (NAGA) with α -galactosidase (GLA) activity as a camouflaged enzyme for putative treatment of Fabry disease (GLA deficiency) (42). Immu-

(AD) model (APP/PS1) mice, could be induced by using AAV gene transfer of transcription factor EB (TFEB), a master regulator of lysosomal degradative pathways, involving upregulation of lysosomal biogenesis and autophagy (46). These findings suggest that not only primary defects of enzymes and functional proteins, but also the secondary dysregulation in metabolic homeostasis, are the main causes of neurodegenerative diseases, including LSDs, PD, and AD due to intracellular accumulation of glycoconjugates, lipids, and proteins, leading to the abnormal functions of organelle and degradative machineries.

Globoid cell leukodystrophy (GCL, also known as Krabbe disease) is another neurodegenerative LSD caused by a deficiency in galactocerebrosidase (GALC) (47). In this disease, the cytotoxic lipid, galactosylsphingosine (psychosine), accumulates in the central nervous system (CNS) and peripheral nervous system. Oligodendrocytes and Schwann cells are particularly sensitive to psychosine, leading to a demyelinating phenotype. Hawkins-Salsbury et al. reported the mechanism-based combination treatment dramatically increases therapeutic efficacy in murine GCL model (twitcher mice), which were simultaneously treated with CNS-directed GT using AAV vector, SRT, and BM transplantation (BMT) to target the primary pathogenic mechanism (GALC deficiency) and 2 consequences of GALC deficiency (psychosine accumulation and neuroinflammation) (47). Therefore, combined therapies for the primary pathogenic cause, as well as for multitargets aggravating the neurological symptoms, will possibly improve therapeutic efficacy for other LSDs with complex pathological and clinical manifestations. We would expect that the GT with the modified *HEXB* and/or intra-CSF ERT using the recombinant mod2B should have more efficient and long-lasting therapeutic effects for neurodegenerative GM2 gangliosidosis in combination with SRT, PCT, and BMT.

In recent years, the molecular imaging with fluorescent probes has been widely applied to monitoring therapy of cancer and other diseases in preclinical studies (12, 48, 49). In this study, we firstly established an enzyme replacement imaging system to visualize the intracellular β -Hex activity of modified HexBs incorporated into living cultured SD fibroblasts with a newly developed fluorescent substrate, HMDER- β GlcNAc specific for the β -Hex, based on the design of previous report (48, 50). We could observe the function (β -Hex activity) and distribution of the modified HexBs in the brain regions of SD mice following the i.c.v. administration to evaluate the therapeutic mechanism of functional recombinant enzymes. Synthetic HMDER derivatives such as fluorogenic substrates will be available for vital imaging of other enzymes in culture and even in vivo systems. An acidic pH-activatable fluorescent probe, AFO, was also utilized to visualize the recombinant lysosomal enzyme delivery to late endosomes/lysosomes in cultured SD fibroblasts by conventional fluorescence microscopy. This fluorescent probe will also be useful for imaging or chase of other lysosomal enzymes and related proteins in acidic cellular compartments (late endosomes/lysosomes). Near-infrared fluorescence molecular imaging of amyloid β species and monitoring therapy in animal models of AD was reported (49). Such monitoring methods with fluorescent probes capable of assisting drug development is highly desirable for monitoring therapy of neurological disorders for not only preclinical studies using animal disease models, but also clinical trials and applications to disease patients.

IMS is a powerful tool that can be used to detect many biomolecules and biological events at the same time, especially for qualitative lipid analysis (14, 16), although it is an invasive technique. Therefore, IMS is also considered useful for monitoring therapy of animal models with neurodegenerative diseases including lipidosis and gangliosidosis. We could validate the reduction of the natural substrates, GM2 and GA2, accumulated in brain regions treated with the modified HexBs by an IMS system. We were able to identify BMP (17, 18) by IMS firstly as another lipid that was remarkably increased in various brain regions, particularly in the CB, of SD mice. The BMP has been reported to form the membranous cytoplasmic body-like (MCB-like) structure with ganglioside at acidic pH in vitro (51). As remarkable accumulation of BMP and GM2 (d20) was observed in the CB of SD mice, the specific colocalization of BMP and GM2 (d20) in MCB-like structure was suggested. Furthermore, the marked reduction of not only GM2 and GA2, but also BMP — which is involved in endosomal sorting and traffic regulation of organelles (52) — in the SD mouse brain regions including HY, LSN, HIP, and CB treated with mod2B by i.c.v. injection was closely correlated with improvements in their motor dysfunction, as evaluated by the rota-rod test. It also led to lifespan extension. Marked reduction of BMP by mod2B replacement but not by modB suggests that mod2B should have more potent GM2-degrading activity in vivo than modB, and BMP was considered to be secondarily reduced corresponding to the decrease of GM2 accumulated in the brain parenchyma. These findings also corresponded with those on behavioral phenotype of SD mice, as previously reported (53). BMP accumulation in the cerebella of the patients is possible to contribute to the cerebellar neurodegeneration leading to the cerebellar atrophy. To the best of our knowledge, this is the first demonstration of the relationship between the therapeutic effects of a treatment and imaging data obtained by IMS. As the contributions of lyso-GM2, phospholipids, and myelin-enriched lipids to the neuropathogenesis of glycosphingolipidosis was suggested (2, 54–56), multitarget validation by IMS for disease-related and therapeutic biomarkers including brain lipids will be very helpful for elucidation of the neuropathogenic mechanism in small animal disease models and monitoring combined drug therapy in preclinical studies. We anticipate that i.c.v.ERT and/or GT utilizing the modified *HEXB* will be subjected to preclinical studies and clinical trials leading to clinical applications for the treatment of TSD patients in the near future not only in high-risk Ashkenazi-Jewish patients, but also in non-Jewish populations worldwide.

Methods

Supplemental Methods are available online with this article.

Animals. SD model mice (*Hexb*^{-/-}; C57BL/6 \times 129sv) (9, 10) were provided by R.L. Proia (National Institute of Diabetes and Digestive and Kidney Diseases, NIH, Bethesda, Maryland, USA). The mice were bred by mating them with C57BL/6 mice (Japan SLC) and were maintained under specific pathogen-free conditions in the animal facilities at Tokushima University.

Antibodies. GM2-specific mouse mAb (GMB28: IgM) (29) was provided by T. Tai (The Tokyo Metropolitan Institute of Medical Science, Tokyo, Japan). Antiserum, anti-NAG(A), against human HexA ($\alpha\beta$ heterodimer) raised in rabbits (30) were provided by A. Tsuji (Graduate School of Advanced Technology and Science and of Biological Science and Technology, Tokushima University).

Cells. The CHO-K1 cell line was provided by RIKEN BioResource Center. The normal skin fibroblast cell line (Hs68) was provided by the Japanese Collection of Research Bioresources Cell Bank. The fibroblasts were cultured in nutrient mixture Ham's F-10 (Sigma-Aldrich) medium containing 10% (v/v) FBS and antibiotics at 37°C in a humidified incubator continuously flushed with a mixture of 5% CO₂ and 95% air.

Establishment of CHO cell lines expressing modB and mod2B. DNA fragments 1 and 2, respectively encoding the modified *HEXB* and *HEXB2*, were amplified using primer sets (Supplemental Table 3), and the previously constructed pCXN₂-modified *HEXB-Neo* vector (5) was used as a template under the indicated conditions (Supplemental Table 3). Both the insert and linearized pCXN₂-*Neo* vector were digested with XhoI and BglII (TOYOBO), then were ligated into the pCXN₂-*Neo* vector with the In-Fusion system (Takara Bio) according to the manufacturer's instructions. The resultant vector plasmid was designated pCXN₂-modified *HEXB2-Neo* and was transformed into MAX Efficiency DH5 α Competent Cells (Invitrogen). Plasmid DNA-Lipofectamine 2000 (Invitrogen) complexes were transfected into CHO cells according to the manufacturer's instructions. Neomycin-resistant cell lines were established by G418 (Sigma-Aldrich) selection and the limiting dilution method.

Enzyme assays. Hex isozymes were diluted with BSA (Sigma-Aldrich) to a final concentration of 0.5 mg/l if needed. Then β -Hex activities toward 4-methylumbelliferyl-6-sulfo-*N*-acetyl- β -D-glucosaminide (MUGS; Merck) were measured in 0.1 M sodium citrate buffer (pH 4.2) (57). The kinetic parameters and in vitro thermostability was analyzed (5, 26). K_m and V_{max} values for 4-MUGS were determined by the method of Lineweaver-Burk plot at various substrate concentrations (0.125–4 mM). Thermostability of modified HexBs were analyzed in 10 mM sodium phosphate buffer (NaPB, pH 6.0) containing 30% SD mice plasma, followed by incubation at 37°C. The protein levels were assayed with the DC Protein Assay or Bio-Rad Protein Assay with BSA as a standard.

X-ray structural study of modB. The modB-containing fraction from HiTrap SP was further purified by gel filtration. A Superdex 200 (10/300) column (GE Healthcare) was equilibrated with PBS, then the single peak at 12.6 ml (~135 kDa) was pooled and concentrated with an Amicon ultra device (30,000 MWCO; Merck Millipore) to 7.2 mg/ml. Rod-shaped clustered crystals were grown from the Index #90 (0.2 M sodium formate, 20% [w/v] PEG 3350) (Hampton Research) condition, and we obtained single crystals by microseeding. The crystals were transferred to cryoprotectant solution (20% [v/v] glycerol, 0.16 M sodium formate, 16% [w/v] polyethylene glycol [PEG] 3350) for 10 seconds and then flash-cooled by liquid nitrogen and stored. The x-ray diffraction data of the modB crystals was collected at beamline AR-NE3a in Photon Factory using a wavelength of 1,000 Å by an ADSC Q270 CCD detector. The crystal was kept at 100 K during the data collection. The data were processed with iMosflm (58), and the molecular replacement solution was calculated by the Molrep software program (58) using the human HexB structure (20) as a search model. The structural refinement was performed by the Refmac5 software program (58), and the model was manually fixed to modB sequences using the Coot program (59). The Ramachandran plot analysis of modB by the Rampage software program (58) showed 465 residues (95.7%) in favored regions, 21 residues (4.3%) in allowed regions, and none in outlier regions. The data collection and the structural refinement statistics are summarized (Supplemental Table 2).

In silico analysis. The x-ray structure of modB and the predicted mod2B model were subjected to an MD simulation to determine the con-

formational differences of the GSEP loop regions between modB (GSEP-LDS) and mod2B (GSEP-SGT) using the Desmond version 3.8 software program (60). To construct the protein structure for mod2B (PDB ID: 5BRO), amino acid substitutions were computationally mutated using Maestro (Schrödinger). The OPLS2005 force field was used for simulations. Initial model structures were placed into TIP3P water molecules solvated with 150 mM sodium chloride. After minimization and relaxation of the model, the production MD phase was performed for 50 ns in an isothermal-isobaric (NPT) ensemble at 300 K and 1 bar using Langevin dynamics. Long-range electrostatic interactions were computed using the smooth particle mesh Ewald method. The structure superposition of MD trajectories and calculation of pairwise RMSD of the GSEP loop region were performed using the MOE program (Chemical Computing Group). All system setups were performed using Maestro. All molecular figures were generated using PyMOL (Schrödinger).

Enzyme replacement assay for GM2 gangliosidosis fibroblasts. Each type of fibroblast was seeded onto a collagen type I-coated 12-well plate (AGC Techno Glass). ModB and mod2B (MUGS-degrading activity, 2 μ mol h⁻¹) were added, followed by incubation for 4 days. The cells were dissociated with trypsin-EDTA (Invitrogen) and sonicated with PBS containing 1% (v/v) nonidet P-40 (NP-40) (Roche Diagnostics)/protease inhibitors. Then, intracellular MUGS-degrading activities were measured. In some experiments, M6P (Sigma-Aldrich) was added to a final concentration of 5 mM. For the analyses of the protease sensitivity, each sample (7.5 μ g of protein) was subjected to SDS-PAGE and immunoblotting with Ab against human HexA and β -actin (A5316, Sigma-Aldrich, 1:5,000 dilution). For Hex activity imaging, SD patient fibroblasts (F572) and Hs68 were seeded onto 8-well Lab-Tek chamber slides (Thermo Fisher Scientific) coated with 0.05% (w/v) atelocollagen (Koken Co.). ModB and mod2B (MUGS-degrading activity, 2 μ mol h⁻¹) were then added, followed by incubation for 24 hours. The cells were treated with HMDER- β -GlcNAc to a final concentration of 20 μ M for 1 hour at 37°C. Nuclei were stained with 10 μ g/ml of bisbenzimidazole H33342 (Sigma-Aldrich). The specimens were viewed with a BIOREVO BZ-9000 device (Keyence). The excitation and emission wavelengths were 540 nm and 605 nm, respectively.

For the Hex delivery imaging, modB and mod2B were mixed with AFO-NHS (Goryo Chemical Inc.) according to the manufacturer's instructions. AFO-NHS, -modB, and -mod2B (each 100 pmol) were added to SD fibroblasts (F572), followed by incubation for 24 hours. The cells were viewed with a LSM700 confocal fluorescent microscope (Zeiss). The excitation and emission wavelengths were 555 nm and 585 nm, respectively.

For immunostaining, TSD fibroblasts (F218) were seeded onto 8-well Lab-Tek chamber slides coated with 0.05% atelocollagen. Then, modB and mod2B (MUGS-degrading activity 2 μ mol h⁻¹) were added, followed by incubation for 4 days. The fibroblasts were fixed with 4% paraformaldehyde. After the samples were washed with PBS, the intracellular GM2 and Hex were detected by Ab against GM2 and human HexA (5). The specimens were viewed with the LSM700. Image analyses were performed using the ZEN2012 program (Zeiss).

For a GM2-ELISA (31), TSD fibroblasts were seeded onto a collagen type I-coated 96-well plate (AGC Techno Glass, 1 \times 10⁴ cells/well). ModB and mod2B (MUGS-degrading activity 1 μ mol h⁻¹) were added, followed by incubation for 7 days. The cells were fixed with 4% (w/v) paraformaldehyde/PBS overnight at 4°C. After washing with PBS, the cells were

treated with 0.6% H₂O₂/PBS for 30 minutes and 5% goat serum/1% (w/v) BSA/PBS at 37°C for 2 hours. They were then immunostained with GM2-specific Ab (1:100 dilution) overnight at 4°C. After washing, the cells were treated with biotin-conjugated Ab against mouse IgG, IgM (Thermo Scientific, 1:1,000 dilution) at room temperature (r.t.) for 1 hour. After washing, the cells were treated with horseradish peroxidase-conjugated (HRP-conjugated streptavidin [Dako, 1:2,000 dilution]) at r.t. for 1 hour. After washing, a peroxidase assay kit for ELISA (Sumitomo Bakelite) was used with a microtiter plate reader at 450 nm.

i.c.v. administration to SD mice. A 1–5 mg/kg BW dose of modB or mod2B, or the same volume of PBS, was injected into 10-week-old SD mice by i.c.v. administration (5). For repeated administration (twice) at 2-week intervals beginning from the age of 10 weeks, the enzyme solutions were injected at the same site in the same manner. One week after the injection, the SD mice were sacrificed, and their brains, livers, and spleens were dissected after PBS perfusion. Each tissue was frozen immediately. The sections were thawed and homogenized by sonication in PBS containing protease inhibitors. After centrifugation at 13,200 g, the supernatants were collected as tissue extracts. The MUGS-degrading activities per wet weight of tissues were calculated.

For immunoprecipitation (IP), protein A-agarose (Bio-Rad) was washed with 1% (v/v) Triton X-100 (Nacalai Tesque)/TBS (25 mM Tris [Sigma-Aldrich], 137 mM NaCl [Nacalai Tesque], 2.7 mM KCl [Sigma-Aldrich]; pH 7.4). After binding with anti-NAG(A) specific for human HexA at 4°C overnight, the brain extracts were treated at r.t. for 2 hours. After washing, the bound Hex proteins were eluted with SDS sample buffer containing 50 mM Tris-HCl (Wako) (pH 6.8), 6% (v/v) glycerol (Wako), 0.2% (v/v) 2-ME (Wako), 4% (w/v) SDS (Sigma-Aldrich), and 0.002% (w/v) bromophenol blue (Kishida Chemical). Each sample was subjected to SDS-PAGE and immunoblotting. The PVDF membranes were treated with human HexA-specific Ab (1:1,000 dilution) and Clean-Blot IP Detection solution (Thermo Scientific, 1:500 dilution). The molecular weight of each recombinant Hex was calculated based on that of the Biotinylated Protein Ladder (Cell Signaling Technology). The Image J software program (version 1.46) (61) was used to quantify the signal intensity.

For IHC, each brain hemisphere was put in O.C.T. compound (Sakura Seiki) at –20°C. Slices (10- μ m thick) were prepared with a Microm HM550 cryostat (Microedge Instruments), which were then placed on silanized slides (Dako). Each slice was treated with human HexA-specific Ab (1:2,000 dilution). The specimens were viewed with a BIOREVO BZ-9000.

IMS. The brain slices (10- μ m thick) of WT and SD mice were thaw-mounted on indium-tin-oxide-coated slide glasses (Matsunami Glass) and kept at –80°C. The tissue sections were brought to r.t., and 9-aminoacridine (Merck) was sublimated onto the sections with 1.5 μ m thickness by an iMLayer device (Shimadzu). Mass spectra were acquired using a mass microscope, a prototype of the iMScope (Shimadzu). The measurements were performed within a mass range of mass-to-charge ratio (m/z) 790–1,300 (positive ion mode) and 850–1,700 (negative ion mode) using scan pitches of 10 μ m and 70 μ m. The number of laser irradiations was 200 shots at each location with a 5- μ m diameter laser beam. Signal assignments were confirmed using MS/MS analyses. Relative abundance of GM2, GA2, and BMP was evaluated by the signal intensity ratio of each peak to phosphatidylinositol (PI, 38:4) or phosphatidylcholine (PC, 34:1), which were selected as reference lipids. Image reconstruction was performed using the Imaging MS Solution version 1.01.02 software program

(Shimadzu). Serial sections were also stained with Mayer's hematoxylin (Muto Pure Chemicals) and eosin Y (Sigma-Aldrich).

Rota-rod test and lifespan analysis. The abilities of the mice to maintain balance on a rotating cylinder were evaluated by the rota-rod test (4). Rota-rod testing and measurement of the BW were performed every week beginning from when the mice were 10 weeks old and continuing until they could no longer walk. The lifespans of the SD mice were evaluated by the Kaplan-Meier method (4).

Statistics. The statistical analyses were performed using the SigmaPlot11 software program (Systat Software). In comparisons of 3 or more groups, we used a one-way ANOVA with a Tukey post-hoc test. We used the 2-tailed unpaired *t* test to compare the protease sensitivities of modB and mod2B. Survival data were compared by a log-rank test with a Holm-Sidak post-hoc test. A *P* value less than 0.05 was considered significant.

Study approval. All experiments were approved by the ethics committee on animal care at Tokushima University and were performed in accordance with institutional guidelines for animal care at Tokushima University. Cultured skin fibroblasts from patients were approved for use by the ethics committee at Tokushima University.

Author contributions

KK, DT, MK, MS, YU, HS, AO, and KI designed the research. KK, YM, ES, CT, NM, KS, TH, DA, and TT performed experiments. KK, YM, ES, NM, TH, DA, TT, and KI analyzed data. KK, NM, TH, MS, YU, and KI wrote the manuscript.

Acknowledgments

We would like to acknowledge the beamline staff at the Photon Factory (Ibaraki, Japan) for supporting the data collection (proposal 2013G075). This work was supported by the Program for Promotion of Fundamental Studied Health Sciences of the National Institute of Biomedical Innovation (NIBIO, grant 09-15); Japan Science and Technology Agency Exploratory Research for Advanced Technology; Platform Project for Supporting Drug Discovery and Life Science Research (Platform for Drug Discovery, Informatics, and Structural Life Science); Project for Creation of Research Platforms and Sharing of Advanced Research Infrastructure (grant. 25801) from the Ministry of Education, Culture, Sports, Science and Technology (MEXT); the Japan Society for the Promotion of Science (JSPS) and the Japan Agency for Medical Research and Development (AMED); and MEXT/JSPS KAKENHI (grants 24659262, 25110722, 25116712, and 25293044).

Address correspondence to: Kohji Itoh, Department of Medicinal Biotechnology, Institute for Medicinal Research, Graduate School of Pharmaceutical Sciences, Tokushima University 1-78 Sho-machi, Tokushima, Tokushima770-8505, Japan. Phone: 81.88.633.7290; E-mail: kitoh@tokushima-u.ac.jp.

Daisuke Asanuma's present address is: Department of Neurobiology, Graduate School of Medicine, The University of Tokyo, Tokyo, Japan.

Kohei Sato's present address is: Department of Applied Chemistry and Biochemical Engineering, Faculty of Engineering, Shizuoka University, Shizuoka, Japan.

1. Gravel RA, et al. The GM2 gangliosidosis. In: Scriver CR, Beaudet AL, Sly WS, Valle D, eds. *The Metabolic and Molecular Bases of Inherited Disease*. New York, New York, USA: McGraw-Hill; 2001:3827–3876.
2. Cachón-González MB, Wang SZ, Ziegler R, Cheng SH, Cox TM. Reversibility of neuropathology in Tay-Sachs-related diseases. *Hum Mol Genet*. 2014;23(3):730–748.
3. Bradbury AM, et al. Therapeutic response in feline Sandhoff disease despite immunity to intracranial gene therapy. *Mol Ther*. 2013;21(7):1306–1315.
4. Tsuji D, et al. Highly phosphomannosylated enzyme replacement therapy for GM2 gangliosidosis. *Ann Neurol*. 2011;69(4):691–701.
5. Matsuoka K, et al. Therapeutic potential of intracerebroventricular replacement of modified human β -hexosaminidase B for GM2 gangliosidosis. *Mol Ther*. 2011;19(6):1017–1024.
6. Platt FM, et al. Prevention of lysosomal storage in Tay-Sachs mice treated with N-butyldeoxyynojirimycin. *Science*. 1997;276(5311):428–431.
7. Maegawa GH, et al. Substrate reduction therapy in juvenile GM2 gangliosidosis. *Mol Genet Metab*. 2009;98(1–2):215–224.
8. Clarke JT, et al. An open-label Phase I/II clinical trial of pyrimethamine for the treatment of patients affected with chronic GM2 gangliosidosis (Tay-Sachs or Sandhoff variants). *Mol Genet Metab*. 2011;102(1):6–12.
9. Sango K, et al. Mouse models of Tay-Sachs and Sandhoff diseases differ in neurologic phenotype and ganglioside metabolism. *Nat Genet*. 1995;11(2):170–176.
10. Sango K, et al. Mice lacking both subunits of lysosomal β -hexosaminidase display gangliosidosis and mucopolysaccharidosis. *Nat Genet*. 1996;14(3):348–352.
11. Hawkes C, Kar S. Insulin-like growth factor-II/mannose-6-phosphate receptor: widespread distribution in neurons of the central nervous system including those expressing cholinergic phenotype. *J Comp Neurol*. 2003;458(2):113–127.
12. Urano Y, et al. Selective molecular imaging of viable cancer cells with pH-activatable fluorescence probes. *Nat Med*. 2009;15(1):104–109.
13. Asanuma D, et al. Acidic-pH-activatable fluorescence probes for visualizing exocytosis dynamics. *Angew Chem Int Ed Engl*. 2014;53(24):6085–6089.
14. Yuki D, et al. DHA-PC and PSD-95 decrease after loss of synaptophysin and before neuronal loss in patients with Alzheimer's disease. *Sci Rep*. 2014;4:7130.
15. Eriksson C, Masaki N, Yao I, Hayasaka T, Setou M. MALDI Imaging Mass Spectrometry — A mini review of methods and recent developments. *Mass Spectrom (Tokyo)*. 2013;2(spec iss):S0022.
16. Chen Y, et al. Imaging MALDI mass spectrometry using an oscillating capillary nebulizer matrix coating system and its application to analysis of lipids in brain from a mouse model of Tay-Sachs/Sandhoff disease. *Anal Chem*. 2008;80(8):2780–2788.
17. Kobayashi T, et al. Late endosomal membranes rich in lysobisphosphatidic acid regulate cholesterol transport. *Nat Cell Biol*. 1999;1(2):113–118.
18. Akgoc Z, Sena-Esteves M, Martin DR, Han X, d'Azzo A, Seyfried TN. Bis(monoacylglycerol) phosphate: A secondary storage lipid in the gangliosidosis. *J Lipid Res*. 2015;56(5):1006–1013.
19. Lemieux MJ, Mark BL, Cherney MM, Withers SG, Mahuran DJ, James MN. Crystallographic structure of human β -hexosaminidase A: interpretation of Tay-Sachs mutations and loss of GM₂ ganglioside hydrolysis. *J Mol Biol*. 2006;359(4):913–929.
20. Mark BL, Mahuran DJ, Cherney MM, Zhao D, Knapp S, James MN. Crystal structure of human β -hexosaminidase B: understanding the molecular basis of Sandhoff and Tay-Sachs disease. *J Mol Biol*. 2003;327(5):1093–1109.
21. Zarghooni M, Bukovac S, Tropak M, Callahan J, Mahuran D. An α -subunit loop structure is required for GM2 activator protein binding by β -hexosaminidase A. *Biochem Biophys Res Commun*. 2004;324(3):1048–1052.
22. Kytzia HJ, Sandhoff K. Evidence for two different active sites on human β -hexosaminidase A. *J Biol Chem*. 1985;260(12):7568–7572.
23. Hasilik A, Neufeld EF. Biosynthesis of lysosomal enzymes in fibroblasts. Synthesis as precursors of higher molecular weight. *J Biol Chem*. 1980;255(10):4937–4945.
24. Weitz G, Proia RL. Analysis of the glycosylation and phosphorylation of the α -subunit of the lysosomal enzyme, β -hexosaminidase A, by site-directed mutagenesis. *J Biol Chem*. 1992;267(14):10039–10044.
25. Pennybacker M, Liessem B, Moczall H, Tiffit CJ, Sandhoff K, Proia RL. Identification of domains in human β -hexosaminidase that determine substrate specificity. *J Biol Chem*. 1996;271(29):17377–17382.
26. Matsuoka K, Tsuji D, Aikawa S, Matsuzawa F, Sakuraba H, Itoh K. Introduction of an N-glycan sequon into HEXA enhances human β -hexosaminidase cellular uptake in a model of Sandhoff disease. *Mol Ther*. 2010;18(8):1519–1526.
27. Kinoshita E, Yamada A, Takeda H, Kinoshita-Kikuta E, Koike T. Novel immobilized zinc(II) affinity chromatography for phosphopeptides and phosphorylated proteins. *J Sep Sci*. 2005;28(2):155–162.
28. Sato K, et al. Total chemical synthesis of monoglycosylated GM2 ganglioside activator using a novel cysteine surrogate. *Chem Commun (Camb)*. 2015;51(49):9946–9948.
29. Kotani M, Ozawa H, Kawashima I, Ando S, Tai T. Generation of one set of monoclonal antibodies specific for α -pathway ganglio-series gangliosides. *Biochim Biophys Acta*. 1992;1117(1):97–103.
30. Izumi T, Fukuyama Y, Tsuji A, Yamanaka T, Hirabayashi Y, Suzuki Y, G_{M2}-Gangliosidosis: B1 variant with thermostable β -hexosaminidase A and molecular analysis of the mutant enzyme. In: Salvayre R, Douste-Blazy L, Gatt S, eds. *Lipid Storage Disorders: Biological and Medical Aspects*. New York, New York, USA: Plenum; 1988:237–245.
31. Tsuji D, Higashine Y, Matsuoka K, Sakuraba H, Itoh K. Therapeutic evaluation of GM2 gangliosidosis by ELISA using anti-GM2 ganglioside antibodies. *Clin Chim Acta*. 2007;378(1–2):38–41.
32. Barton NW, et al. Replacement therapy for inherited enzyme deficiency—macrophage-targeted glucocerebrosidase for Gaucher's disease. *N Engl J Med*. 1991;324(21):1464–1470.
33. Beard H, et al. Determination of the role of injection site on the efficacy of intra-CSF enzyme replacement therapy in MPS IIIA mice. *Mol Genet Metab*. 2015;115(1):33–40.
34. Vuilleminot BR, et al. Recombinant human tripeptidyl peptidase-1 infusion to the monkey CNS: safety, pharmacokinetics, and distribution. *Toxicol Appl Pharmacol*. 2014;277(1):49–57.
35. Vera M, et al. Immune response to intrathecal enzyme replacement therapy in mucopolysaccharidosis I patients. *Pediatr Res*. 2013;74(6):712–720.
36. Muenzer J, et al. A phase I/II study of intrathecal idursulfase-IT in children with severe mucopolysaccharidosis II. *Genet Med*. 2016;18(1):73–81.
37. Meng Y, et al. Effective intravenous therapy for neurodegenerative disease with a therapeutic enzyme and a peptide that mediates delivery to the brain. *Mol Ther*. 2014;22(3):547–553.
38. Tardieu M, et al. Intracerebral administration of adeno-associated viral serotype rh.10 carrying human *SGSH* and *SUMF1* cDNAs in children with mucopolysaccharidosis type IIIA disease: results of a phase I/II trial. *Hum Gene Ther*. 2014;25(6):506–516.
39. Wang J, et al. Neutralizing antibodies to therapeutic enzymes: considerations for testing, prevention and treatment. *Nat Biotechnol*. 2008;26(8):901–908.
40. Nielsen M, et al. Reliable prediction of T-cell epitopes using neural networks with novel sequence representations. *Protein Sci*. 2003;12(5):1007–1017.
41. Rammensee H, Bachmann J, Emmerich NP, Bachor OA, Stevanović S. SYFPEITHI: database for MHC ligands and peptide motifs. *Immunogenetics*. 1999;50(3–4):213–219.
42. Tajima Y, et al. Use of a modified α -N-acetylgalactosaminidase in the development of enzyme replacement therapy for Fabry disease. *Am J Hum Genet*. 2009;85(5):569–580.
43. Sinici I, et al. In cellulo examination of a β - α hybrid construct of β -hexosaminidase A subunits, reported to interact with the GM2 activator protein and hydrolyze GM2 ganglioside. *PLoS One*. 2013;8(3):e57908.
44. Orenstein SJ, et al. Interplay of LRRK2 with chaperone-mediated autophagy. *Nat Neurosci*. 2013;16(4):394–406.
45. Wong E, Cuervo AM. Autophagy gone awry in neurodegenerative diseases. *Nat Neurosci*. 2010;13(7):805–811.
46. Xiao Q, et al. Neuronal-targeted TFEB accelerates lysosomal degradation of APP, reducing A β generation and amyloid plaque pathogenesis. *J Neurosci*. 2015;35(35):12137–12151.
47. Hawkins-Salsbury JA, et al. Mechanism-based combination treatment dramatically increases therapeutic efficacy in murine globoid cell leukodystrophy. *J Neurosci*. 2015;35(16):6495–6505.
48. Asanuma D, et al. Sensitive β -galactosidase-targeting fluorescence probe for visualizing small peritoneal metastatic tumours in vivo. *Nat Commun*. 2015;6:6463.
49. Zhang X, et al. Near-infrared fluorescence molecular imaging of amyloid beta species and monitoring therapy in animal models of Alzheimer's disease. *Proc Natl Acad Sci U S A*. 2015;112(31):9734–9739.

50. Kamiya M, et al. β -Galactosidase fluorescence probe with improved cellular accumulation based on a spirocyclized rhodol scaffold. *J Am Chem Soc.* 2011;133(33):12960–12963.
51. Hayakawa T, et al. pH-dependent formation of membranous cytoplasmic body-like structure of ganglioside G(M1)/bis(monoacylglycerol) phosphate mixed membranes. *Biophys J.* 2007;92(1):L13–L16.
52. Konishi Y, Setou M. Tubulin tyrosination navigates the kinesin-1 motor domain to axons. *Nat Neurosci.* 2009;12(5):559–567.
53. Hu L, Sun Y, Villasana LE, Paylor R, Klann E, Pautler RG. Early changes in the apparent diffusion coefficient (ADC) in a mouse model of Sandhoff's disease occur prior to disease symptoms and behavioral deficits. *Magn Reson Med.* 2009;62(5):1175–1184.
54. Neuenhofer S, Conzelmann E, Schwarzmann G, Egge H, Sandhoff K. Occurrence of lysoganglioside lyso-GM2 (II3-Neu5Ac-gangliotriaosylsphingosine) in GM2 gangliosidosis brain. *Biol Chem Hoppe Seyler.* 1986;367(3):241–244.
55. Buccoliero R, Bodennec J, Van Echten-Deckert G, Sandhoff K, Futerman AH. Phospholipid synthesis is decreased in neuronal tissue in a mouse model of Sandhoff disease. *J Neurochem.* 2004;90(1):80–88.
56. Baek RC, Martin DR, Cox NR, Seyfried TN. Comparative analysis of brain lipids in mice, cats and humans with Sandhoff disease. *Lipids.* 2009;44(3):197–205.
57. Suzuki K. Enzymatic diagnosis of sphingolipidoses. *Methods Enzymol.* 1987;138:727–762.
58. Winn MD, et al. Overview of the CCP4 suite and current developments. *Acta Crystallogr D Biol Crystallogr.* 2011;67(pt 4):235–242.
59. Emsley P, Lohkamp B, Scott WG, Cowtan K. Features and development of Coot. *Acta Crystallogr D Biol Crystallogr.* 2010;66(pt 4):486–501.
60. Bowers KJ, et al. Scalable algorithms for molecular dynamics simulations on commodity clusters. Presented at: SC '06 Proceedings of the 2006 ACM/IEEE conference on Supercomputing; November 11–17, 2006; Tampa, Florida, USA. Article 84.
61. Schneider CA, Rasband WS, Eliceiri KW. NIH Image to ImageJ: 25 years of image analysis. *Nat Methods.* 2012;9(7):671–675.